Articles

Size Particle Effects on Lithium Insertion into Sn-doped TiO_2 Anatase

L. Aldon,* P. Kubiak, A. Picard, J.-C. Jumas, and J. Olivier-Fourcade

Laboratoire des Agrégats Moléculaires et Matériaux Inorganiques, UMR 5072 CNRS, cc 015, Université Montpellier II, Place Eugène Bataillon, 34095 Montpellier Cedex 5, France

Received July 4, 2005. Revised Manuscript Received December 13, 2005

Lithium insertion into Sn-doped TiO_2 anatase was studied in order to clarify the mechanism responsible for the first plateau observed at 1.75 V vs Li. One of the other aims of this study was to get deeper insight into the process responsible for the appearance of a first domain observed at a small amount of lithium (before the plateau) and a third domain between 1.7 and 1.2 V (after the plateau). Pure and Sn-substituted anatase were synthesized by several synthetic methods with different precursors and solvents. These materials are expected to have different electrochemical properties because crystallite size modifies the Li-insertion process. Their electrochemical behavior is discussed in order to establish a relationship between the materials properties and the electrochemical performances. Three processes have been identified from both X-ray diffraction and ^{119}Sn Mössbauer spectroscopy: (i) topotactic insertion into the Li-poor compound Li_xTiO_2, with the x value depending on the particle size; (ii) a two-phase system mechanism leading to the phase transition Li_xTiO_2 (Anatase, $I4_1/amd$) → Li_yTiO_2 (orthorhombic distortion, *Imma*); and (iii) another topotactic insertion into the Li-rich compound Li_yTiO_2. Crystallite size governs the topotactic mechanism but does not improve the overall electrochemical capacity of the material.

Introduction

Anodic materials with a discharge potential of about 1 V/Li are chosen from among the titanium oxides. The mechanism is based on the redox couple Ti^{4+}/Ti^{3+} working at approximately 1.5 V relative to lithium. The materials tested up to now are all Ti^{4+} oxides. Several families can be distinguished: (i) The TiO_2 stable phases with various polymorphs (anatase,[1] rutile[2]) more or less modified by doping. Anatase is the only form of TiO_2 that gives satisfactory electrochemical performances.[3−5] (ii) The TiO_2 metastable phases obtained by mechanical grinding (TiO_2-(II), ixiolite/srilankite/brookite)[6,7] or by chemical extraction of cations from more-complex ternary compounds such as hollandite ($K_xTi_8O_{16}$)[8−10] or ramsdellite ($Li_xTi_2O_4$, $0 < x < 1$).[11−13]

The introduction of an element with a charge state lower or higher than that of the titanium ion in small amounts modifies the number of free charge carriers and thus the[13] electronic conduction properties. An element in a higher charge state leads to the reduction of a fraction of Ti^{4+} to Ti^{3+}; an element with a lower charge state (Fe^{3+})[14] creates vacancies in the oxygen sublattice.[15,16] In this way, we obtain n- or p-doped materials, respectively. The creation of vacancies also improves the ionic conductivity.

Substitution by an element with the same charge state as Ti (Zr, Sn) may have several consequences: (i) extension of the domain of stability of a given polymorph (this is the case for Zr-doped anatase, which is more stable at higher temperatures than pure anatase);[17,18] (ii) modification of the particle size by a nucleation effect,[19] which also means a

* To whom correspondence should be addressed. E-mail: laldon@univ-montp2.fr

(1) Horn, M.; Schwerdtfeger, C. F.; Meagher, E. P.; *Z. Kristallogr.* **1972**, *136*, 273.
(2) Meagher, E. P.; George, A. L. *Can. Mineral.* **1979**, *17*, 77.
(3) Huang, S. Y.; Kavan, L.; Exnar, I.; Grätzel, M. *J. Electrochem. Soc.* **1995**, *142*, L142.
(4) Zachau-Christiansen, B.; West, K.; Jacobsen, T.; Atlung, S. *Solid State Ionics* **1988**, *28−30*, 1176.
(5) Ohzuku, T.; Kodama, T.; Hirai, T. *J. Power Sources* **1985**, *14*, 61.
(6) Suryanarayana, C. *Prog. Mater. Sci.* **2001**, *46*, 1−184.
(7) Begin-Colin, S.; Girot, T.; Mocellin, A.; Le Caër, G. *Nanostruct. Mater.* **1999**, *12*, 195−198.
(8) Sasaki, T.; Watanabe, M.; Fujiki, Y. *Acta Crystallogr., Sect. B* **1993**, *49*, 838.
(9) Watanabe, M.; Komatsu, Y.; Sasaki, T.; Fujiki, Y. *J. Solid State Chem.* **1991**, *92*, 80.
(10) Noailles, L. D.; Johnson, C. S.; Vaughey, J. T.; Thacheray, M. M. *J. Power Sources* **1999**, *81−82*, 259.
(11) Akimoto, J.; Gotoh, Y.; Oosawa, Y.; Nonose, N.; Kumagai, T.; Aoki, K. *J. Solid State Chem.* **1994**, *113*, 27.
(12) Kuhn, A.; Amandi, R.; Garcia-Alvarado, F. *J. Power Sources* **2001**, *92*, 221.
(13) Gover, R. K. B.; Tolchard, J. R.; Tukamato, H.; Murai, T.; Irvine, J. T. S. *J. Electrochem. Soc.* **1999**, *146*, 4348.
(14) Lee, H. M.; Kim, S. J.; Shim, I.; Kim, C. S. *J. Magn. Magn. Mater.* **2004**, *272−276*, 1565.
(15) Dutta, H.; Sahu, P.; Pradhan, S. K.; De, M. *Mater. Chem. Phys.* **2002**, *9305*, 1.
(16) Rodriguez-Talavera, R.; Vargas, S.; Arroyo-Murillo, R.; Montiel-Campos, R.; Haro-Poniatowski, E. *J. Mater. Res.* **1997**, *12*, 439.
(17) Mao, D.; Lu, G.; Chen, Q. *Appl. Catal., A* **2004**, *263*, 83.
(18) Hirano, M.; Nakahara, C.; Ota, K.; Tanaike, O.; Inagaki, M. *J. Solid State Chem.* **2003**, *170*, 39.

10.1021/cm051445v CCC: $33.50
Published on Web 02/17/2006

more-rapid formation of the desired phase and improved diffusion rates for the lithium insertion/extraction mechanism. In the batteries, the key issue is the understanding of the nanostructuration of the particles because electrochemical properties are very sensitive to both particle size and the connectivity of the particles due to porosity.

In the present paper, we investigate the influence of the partial substitution of titanium by tin into the anatase framework and the effect of the particle size on the electrochemical behavior. A structural analysis by X-ray diffraction, ^{119}Sn Mössbauer spectroscopy of the tin-doped phase, and a fine analysis of the electrochemical mechanism have allowed us to establish a relationship between structure and electrochemical properties.

Experimental Section

Synthetic Process. Synthetic routes from sol−gel processes have been investigated with different precursors in order to obtain the anatase form of TiO_2. It is prepared by the hydrolysis of either $TiCl_4$ or titanium isopropoxide and various dopant precursors. The precipitates are annealed at 450 °C under air. The insertion mechanism has been investigated for five samples of anatase: (a) a commercial sample provided by Aldrich has been analyzed for comparison; (b) and a 5% tin-doped sample prepared by precipitation from $TiCl_4$ and $SnCl_4$ with $5H_2O$ in ethanol; (c and d) undoped TiO_2 anatase obtained from the hydrolysis of $TiCl_4$ by either H_2O or EtOH, and finally (e) hydrolysis of the organic precursor Ti(OiPr)$_4$ by EtOH. The various synthetic routes gave different crystallite sizes, as deduced from the broadening of the X-ray diffraction line, that have been correlated to the topotactic mechanism during electrochemical insertion into these compounds.

X-ray Diffraction. Pristine and lithiated samples were characterized by X-ray Powder Diffraction (XPD) with a Philips $\theta-2\theta$ diffractometer using Cu Kα radiation ($\lambda = 1.5418$ Å) and a nickel filter. Particle size effects were studied in order to correlate them with electrochemical performances. To this end, we have determined the size of the X-ray coherent domains from the width of the powder diffraction peaks using the fundamental parameters approach proposed by Cheary and Coelho.[20] This procedure is based on the Scherrer method using the full width at half-maximum of the broadened peaks and taking into account experimental broadening due to instruments. Calibration of this procedure has been done with high-quality polycrystalline Si. Crystallographic reference data for the TiO_2 anatase were taken from International Tables for Crystallography (JCPDS No. 21-1272, $a = 3.785$ Å and $c = 9.514$ Å) and were used in the initial stages of refinement of the cell parameters. Because of the cell distortion induced by lithium insertion, the TiO_2 anatase structure usually described in the tetragonal space group $I4_1/amd$ was refined in the orthorhombic *Imma* space group.

Electrochemical Tests. For the five samples, electrochemical lithiations were carried out with (Li/LiPF6 1 M (EC:DMC)/TiO2 anatase) Swagelok test cells as described in ref 21.[21] Galvanostatic discharge/charge curves were obtained with a cycling rate of 1 Li/15 h (C/15). Electrochemical charge/discharge cycles were carried out at 2.5 A/kg and stopped at several characteristic points on the curve. The tin-doped samples were then extracted from the test cell and examined by ex situ X-ray diffraction under inert atmosphere conditions and by ^{119}Sn Mössbauer spectroscopy.

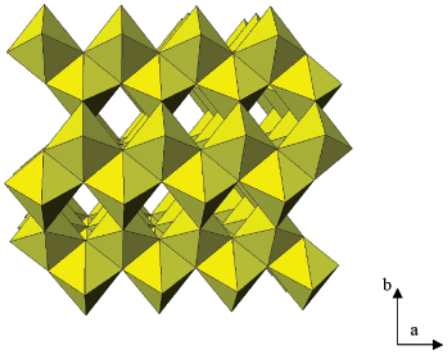

Figure 1. Crystal structure representation showing the one-dimensional channel where lithium atoms can be inserted into the TiO_2 anatase[1].

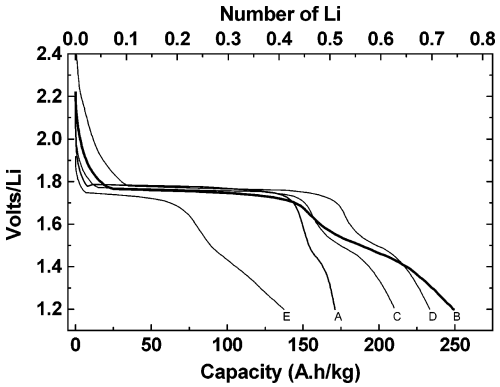

Figure 2. Cell voltage as a function of the number of inserted lithium (discharge) and extracted lithium (charge) ions. Tin-doped sample B presents a lower potential plateau, smaller polarization, and higher capacity than commercial TiO_2 anatase (sample A). Li ion dynamics are influenced by sizing down nanoparticles, as shown and expected for these materials.

^{119}Sn Mössbauer Spectroscopy. Tin-doped anatase and some samples at several depths of discharge and charge have been characterized by ^{119}Sn Mössbauer spectroscopy at room temperature in a transmission mode with a classical EG&G constant acceleration spectrometer. The γ-ray source was Ba^{119m}SnO$_3$. The velocity scale was calibrated with the magnetic sextet spectrum of a high-purity iron foil absorber and ^{57}Co(Rh) as source. Samples have been studied in a specific sample holder. The isomer shifts are given relative to $BaSnO_3$ used as the standard reference. For the electrochemically inserted samples, the measurements were performed ex situ from Swagelok electrodes. All spectra were fitted to Lorentzian profiles by the least-squares method,[22] and the fit was quality controlled by the usual χ^2 and misfit tests.

Results

Electrochemical Behavior. TiO_2 anatase has been extensively studied, and its crystal structure is well-known.[1] It is composed of distorted TiO_6 octahedra and shows large channels, favoring the insertion of lithium as shown in Figure 1. For clarity, we have shown in Figure 2 the first discharge curves of the five studied samples. For sample B, substitution of 5 at % Ti by Sn does not significantly change the capacity of the working voltage, the latter still being around 1.75 V vs Li.

Sample A presents a reversible capacity of 145 Ah kg^{-1}, whereas tin-doped sample B has a reversible capacity of 198

(19) Wagemaker, M.; Kearley, G. J.; van Well, A. A.; Mulka, H.; Mulder, F. M. *J. Am. Chem. Soc.* **2003**, *125*, 840.
(20) Cheary, R. W.; Coelho, A. A. *J. Appl. Crystallogr.* **1992**, *25*, 109.
(21) Denis, S.; Baudrin, E.; Touboul, M.; Tarascon, J. M. *J. Electrochem. Soc.* **1997**, *144*, 4099.
(22) Ruebenbauer, K.; Birchall, T. *Hyperfine Interact.* **1979**, *7*, 125.

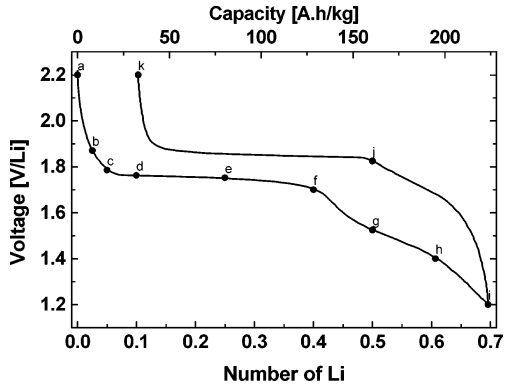

Figure 3. Cell voltage as a function of the number of lithium ions inserted or extracted in tin-doped TiO_2 showing different discharge/charge depths (a−k) for ex situ characterizations (X-ray diffraction and ^{119}Sn Mössbauer spectroscopy).

Ah kg^{-1}. The two TiO_2 samples synthesized from $TiCl_4$ (C and D) show good electrochemical performances during the first discharge. The reversible capacity is about 204 Ah kg^{-1} for anatase formed in aqueous media (C) and about 159 Ah kg^{-1} for that synthesized in alcoholic media (D). In the latter case, we observe a great loss of capacity at the end of the first cycle (75 Ah kg^{-1}). Anatase obtained from titanium isopropoxide (E) shows poor performances. Its reversible capacity is about 106 Ah kg^{-1}. These results are due to the weak extension of the first plateau and the second S-shaped domain. In the case of undoped TiO_2 anatase, electrochemical discharge curves (see Figure 2) show three distinct domains involving two mechanisms: a decrease in the voltage until a lithium content limit (x_{lim}) is reached, a plateau at about 1.75 V (0.07−0.5 inserted Li) attributed to a two-phase system (I), and an S-shaped curve ranging from 1.75 to 1.2 V that corresponds to a one-phase system (II). Depending on the crystallite size for various synthesis conditions, the length of the plateau and the first discharge capacity present an optimum for a crystallite size of about 157 Å. Synthesized tin-doped sample B, with a crystallite size of about 126 Å, presents rather good electrochemical performances.

In addition, because sample B and others have different chemical compositions, it is very difficult to discuss their electrochemical behavior in terms of crystallite size. Other properties such as electric conductivity should also be taken into account.

For sample B, we have chosen several discharge and charge depths for characterization in order to get deeper insight into the lithium insertion extraction mechanism. As indicated in Figure 3, we have examined the samples by ex situ X-ray diffraction under inert atmosphere conditions and by ^{119}Sn Mössbauer spectroscopy.

Structural Characterization. Table 1 gives correspondences with lithiated and unlithiated TiO_2 described in the same space group. Cell parameter refinements have been summarized in Table 2. As an example of line broadening of the X-ray diffraction lines, Figure 4 shows differences for the tin-doped sample and commercial anatase. Pristine tin-doped material (B) shows a crystallite size smaller than that obtained from commercial deliverers. As can be seen in Figure 5, the fundamental process responsible for the first plateau in both pure and tin-doped anatase is the phase

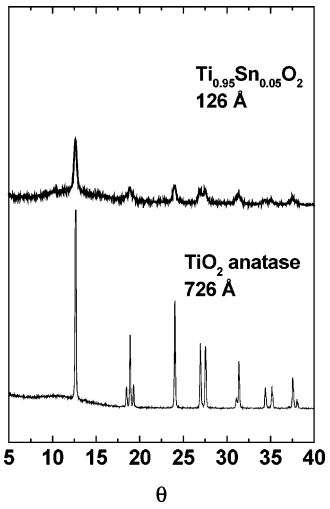

Figure 4. X-ray diffraction patterns of commercial TiO_2 anatase (thin line) and the tin-doped TiO_2 sample (thick line). Crystallite sizes have been estimated with the Scherrer method from the width of diffraction peaks to be about 726 and 126 Å, respectively.

Table 1. Crystallographic Data of TiO_2 Anatase Described in Its Conventional Tetragonal Space Group $I4_1/amd$ and in the Same Orthorhombic Space Group as $Li_{0.5}TiO_2$ for Comparison

atom	Wyckoff site	*x*	*y*	*z*
	TiO_2 anatase, space group $I4_1/amd$[a]			
Ti	4a	0	0	0
O	8e	0	0	0.2079
vacant site	4b	0	0	0.5
	TiO_2 anatase, space group *Imma*			
Ti	4e	0	1/4	0.8741
O_1	4e	0	1/4	0.0888
O_2	4e	0	1/4	0.6685
	$Li_{0.5}TiO_2$, space group *Imma*[c]			
Ti	4e	0	1/4	0.8870
O_1	4e	0	1/4	0.1030
O_2	4e	0	1/4	0.6521
Li	4e	0	1/4	0.3430

[a] Cell parameters: $a = 3.785$Å, $c = 9.514$Å. [b] Cell parameters $a = 3.785$Å, $b = 3.785$Å, $c = 9.514$Å. [c] Cell parameters: $a = 3.806$ Å, $b = 4.073$ Å, $c = 9.047$ Å.

Table 2. Crystallographic Data and Electrochemical Performances of Undoped and Sn-Doped TiO_2 Anatase

sample	*a* (Å)	*b* (Å)	*c* (Å)	x_{lim}	S_{BET} (m^2/g)	L_{coh} (Å)	Q1 (Ah kg^{-1})
A	3.785(2)		9.518(6)	0.024	11.4	726	170
C	3.781(2)		9.487(6)	0.086	79.6	212	224
D	3.782(2)		9.483(6)	0.104	127.8	157	232
E	3.781(2)		9.484(6)	0.020	90	196	137
B	3.796(2)	4.026(3)	9.544(5)	0.071	237.2	126	250
(a) $Li_{0.025}$	3.754(2)	4.027(3)	8.976(7)			104	
(b) $Li_{0.05}$	3.745(3)	4.071(4)	8.978(5)			109	
(g) $Li_{0.5}$	3.828(3)	4.094(4)	9.070(6)			86	
(h) $Li_{0.61}$	3.855(2)	4.049(3)	8.998(6)			69	
(i) $Li_{0.69}$	3.897(3)		9.023(6)			65	

transition from tetragonal anatase to orthorhombic $Li_{0.5}TiO_2$, with a theoretical limit of 167 Ah kg^{-1} in capacity.[23,24] The structure of orthorhombic $Li_{0.5}TiO_2$ is very similar to that of anatase (same TiO_6 octahedra connectivity with Li located in one-half of the interstitial sites of the anatase structure (Ti in 4a, Li in vacant 4b, and O in 8e of the $I4_1/amd$ space

(23) Ebina, T.; Iwasaki, T.; Onodera, Y.; Hayashi, H.; Nagase, T.; Chatterjee, A.; Chiba, K. *J. Power Sources* **1999**, *81−82*, 393.
(24) Zachau-Christiansen, B.; West, K.; Jacobsen, T.; Skaarup, S. *Solid State Ionics* **1992**, *53−56*, 364.

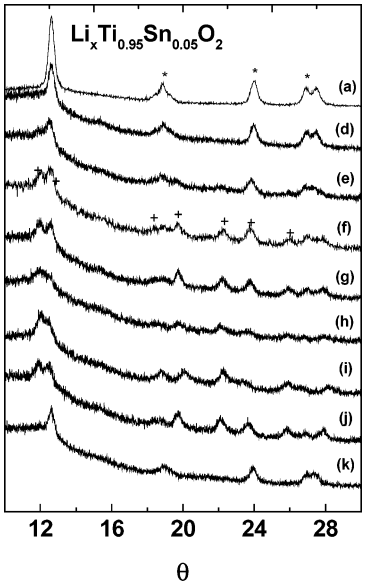

Figure 5. X-ray diffraction patterns of tin-doped TiO_2 sample B (a) before and (d−i) during electrochemical Li insertion and (h−k) extraction. Stars and crosses denote diffraction peaks of an anatase-like structure (tetragonal) and $Li_{0.5+x}TiO_2$ phase (orthorhombic), respectively.

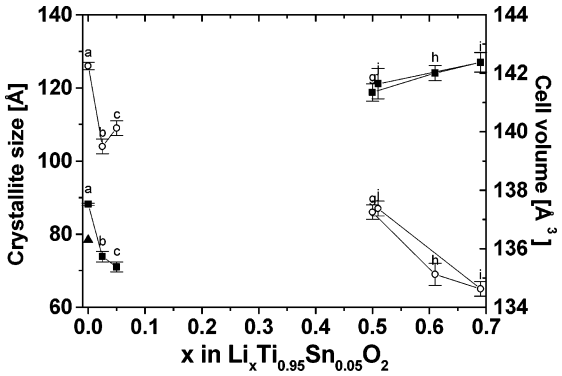

Figure 6. Evolution of the crystallite sizes estimated from the width of diffraction peaks (open circles, left axis) and the cell volume calculated from peak positions (solid squares, right axis) as a function of the amount of Li in tin-doped TiO_2. Solid triangle is drawn for comparison and corresponds to the cell volume of the undoped TiO_2 anatase.

group)). Beyond the first plateau, and beyond 0.5 Li inserted (a → e → f), formation of the orthorhombic phase continues, although we still observe the presence of anatase. This means that Li insertion into $Li_{0.5}TiO_2$ must take place to some extent with the formation of a Li-rich phase Li_xTiO_2.

Figure 6 shows the evolution of the crystallite size and cell volume upon increasing the lithium content. At first, a decrease is seen in the crystallite size during the formation of $Li_{0.5}TiO_2$. This is followed by growth of the newly formed phase. For $x > 0.5$, $Li_{0.5}TiO_2$ reacts with lithium, and the result is a decrease in crystallite size. Figure 6 clearly shows that lithium insertion induced a contraction of the cell in the early stages until $x < 0.07$, at which point the volume expansion results in a variation of about 3.6%. This value is less than that of 4.3% reported for the ramsdellite form of TiO_2.[11] This small swelling explains the good cyclability of this compound. On the other hand, a decrease in the crystallite size with increasing lithium content is in agreement with the core−shell model, because topotactic insertion begins at the surface of these rather small crystallites. Thus,

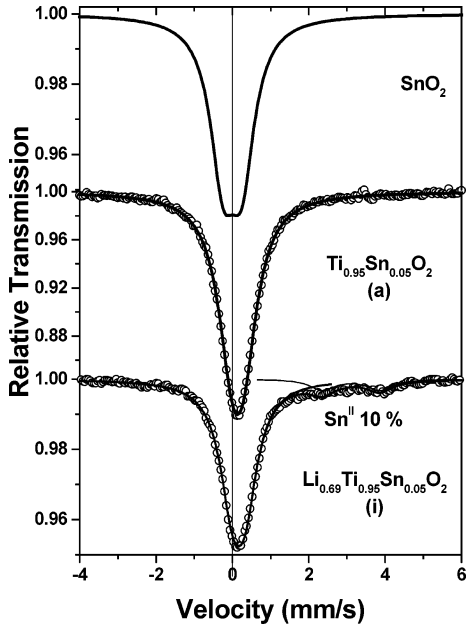

Figure 7. ^{119}Sn Mössbauer spectra of tin-doped TiO_2 (a) before Li insertion and for sample (i) of Figure 3. Partial reduction of Sn^{IV} to Sn^{II} is observed during Li insertion. Spectrum of the SnO_2 cassiterite ($\delta = 0$ mm s^{-1} and $\Delta = 0.03$ mm s^{-1}) with a rutile structure is given as a proof that ^{119}Sn atoms are well-located in Ti sites of the TiO_2 anatase structure because the hyperfine parameters are different ($\delta = 0.03$ mm s^{-1} and $\Delta = 0.32$ mm s^{-1}).

this perturbed surface does not contribute to X-ray diffraction, and only the remaining core still gives a broadened signal in the diffraction pattern. Finally, the deformation of the anatase structure estimated from X-ray diffraction patterns is reversible upon discharge/charge (insertion/deinsertion of lithium). From these experimental results, we found no hysteretic variation of unit cell volume with the lithium insertion and removal process for this tin-doped compound.

Mössbauer Spectroscopy. Examples of ^{119}Sn Mössbauer spectra are shown in Figure 7 for SnO_2 with the rutile structure,[25,26] $Ti_{0.95}Sn_{0.05}O_2$ before lithium insertion, and $Li_{0.69}Ti_{0.95}Sn_{0.05}O_2$ at the end of the discharge. The hyperfine parameters measured by ^{119}Sn Mössbauer spectroscopy, isomer shift δ and quadrupole splitting Δ, reflect changes in the oxidation state and the local environment of the tin atom, respectively, as shown in Table 3. ^{119}Sn Mössbauer spectra allow us to determine the oxidation states of the corresponding cations in the host lattice (Sn^{IV}/Sn^{II}). Substitution of Ti by Sn in the anatase lattice is possible within a limit of 10 at % Sn. Beyond 10 at % Sn, the appearance of SnO_2 as an impurity phase (cassiterite, rutile isomorph) is seen by X-ray diffraction. Mössbauer spectroscopy reveals the presence of Sn^{IV} on octahedral sites, as shown in Figure 7, with hyperfine parameters that differ from those observed for SnO_2 (rutile). This is evidence that tin is located in the titanium crystallographic sites in the anatase structure.

The topotactic domain (a−d) is larger for the tin-doped than for the pure anatase. Mössbauer spectroscopy shows that, at the beginning of the charge/discharge cycle (d), about 10% of the tin is reduced to Sn^{II}. This fraction remains

(25) Hightower, A.; Delcroix, P.; Le Caër, G.; Huang, C−K.; Ratnakumar, B. V.; Ahn, C. C.; Fultz, B. *J. Electrochem. Soc.* **2000**, *147*, 1.
(26) Yamanaka, T.; Kato, A. *Am. Mineral.* **1976**, *61*, 260.

Table 3. ^{119}Sn Mössbauer Parameters Obtained during the First Electrochemical Cycle (values for SnO and SnO_2 given for comparison)

sample	δ (mm/s)	Δ (mm/s)	Γ (mm/s)	contribution	attribution
pristine (a)	0.03(1)	0.32(1)	0.88(8)	100	Sn^{IV}
(d) Li = 0.1	0.03(1)	0.24(2)	0.79(1)	88(2)	Sn^{IV}
	3.20(3)	1.41(4)	0.79(1)	12(2)	Sn^{II}
(e) Li = 0.25	0.02(1)	0.25(2)	0.76(1)	89(2)	Sn^{IV}
	3.17(3)	1.33(4)	0.76(1)	11(2)	Sn^{II}
(f) Li = 0.4	0.02(1)	0.24(2)	0.73(2)	91(2)	Sn^{IV}
	3.29(5)	1.55(7)	0.73(2)	9(2)	Sn^{II}
(g) Li = 0.5	0.01(1)	0.26(2)	0.75(2)	90(2)	Sn^{IV}
	3.11(4)	1.50(6)	0.75(2)	10(2)	Sn^{II}
(h) Li = 0.6	0.04(1)	0.30(1)	0.68(2)	93(2)	Sn^{IV}
	3.13(6)	1.82(8)	0.68(2)	7(2)	Sn^{II}
(i) Li = 0.7	0.05(1)	0.34(1)	0.79(1)	90(2)	Sn^{IV}
	3.00(3)	1.50(4)	0.79(1)	10(2)	Sn^{II}
(j) Li = 0.5	0.02(1)	0.26(1)	0.74(1)	91(2)	Sn^{IV}
	3.17(4)	1.57(5)	0.74(1)	9(2)	Sn^{II}
(k) Li = 0.1	0.02(1)	0.26(1)	0.76(1)	93(2)	Sn^{IV}
	3.08(4)	1.47(5)	0.76(1)	7(2)	Sn^{II}
SnO	2.65	1.35	0.91		refs 27, 28
SnO_2	0.00	0.40			ref 26

constant throughout the cycle. We think that a passivation layer is formed at the surface of the particles, meaning this species is not involved in the cycling process and thus is not directly responsible for the second topotactic domain (f−i) after the plateau. In addition, hyperfine parameters (δ = 3.2(2) mm s^{-1} and Δ = 1.5(3) mm s^{-1}) are significantly different from those usually observed[27] for SnO (δ = 2.65 mm s^{-1} and Δ = 1.35 mm s^{-1}).[28,29] The larger quadrupole splitting agrees with Sn^{II} being surrounded with Ti, Li, and O in the passivation layer. The observed values are not sensitive to the amount of tin (5 and 10%) used for the fitting procedure. Only the χ^2 and misfit tests are changed; positions of the absorption lines are not influenced. The presence of tin, however, reduces the mean crystallite size and extends the insertion range.

Discussion

For undoped TiO_2, crystallite size effects were studied in order to correlate them to electrochemical performances. Because of the different synthesis methods used in this work, we clearly see that crystallite size plays a key issue in the kinetics for the lithium insertion. Depending on the synthetic conditions, the lithium content limit (x_{lim} in Table 2) in the first topotactic domain varies with the capacity determined at 1.2 V during the first discharge. To verify this, we have determined the size of the X-ray coherent domains from the width of the powder diffraction patterns of undoped and tin-doped TiO_2 samples. Pristine samples (doped and undoped) show a pure anatase phase. There are only small differences in lattice parameters and crystallite sizes, but the samples' electrochemical performances are quite different, as shown in Table 2.

For undoped samples, the textural (crystallite size, porosity, BET surface areas) differences can explain the electrochemical performances shown in Figure 8. The commercial anatase presents the biggest crystallite size and does not show the third domain in the discharge curve. Good electrochemical performances for sample B can be explained by its particle size and specific surface area (S_{BET} = 237 m^2 g^{-1}). But we also have to consider differences in chemical composition for sample B because the presence of tin may affect the electronic conductivity of this material. This sample presents a rather good reversible specific capacity of about 198 Ah kg^{-1}. The shape of the electrochemical insertion of Li into Sn-doped anatase is similar to the shape of the electrochemical curve of the pure anatase. These parameters stay constant during the two-phase plateau (d−f) mechanism and vary during the topotactic insertion. It remains an important polarization, which can be avoided by optimizing the carbon black/active mass ratio, and the voltage of the plateau is not modified by tin doping.

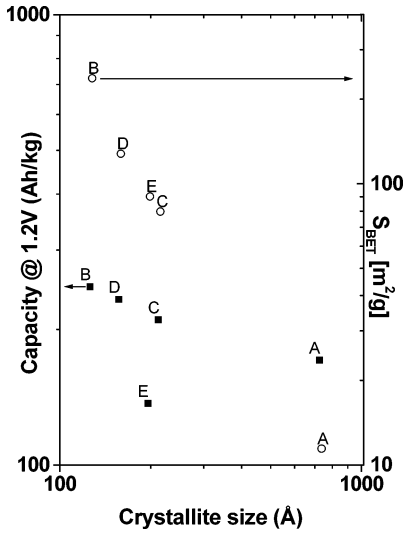

Figure 8. Solid squares represent the capacity of the first discharge at 1.2 V/Li as a function of crystallite size determined from XRD patterns. Open circles represent the specific surface areas of the samples.

^{119}Sn Mössbauer studies clearly demonstrate that Sn atoms are well-substituted in the Ti network. The isomer shift and the quadrupole splitting are sensitive to Li content during insertion. The occurrence of tin II at the beginning of the redox process may be involved in the passivation layer. The contribution of this tin II remains constant, suggesting that it is inactive upon cycling for the studied potential window. The main contribution due to tin IV shows a quadrupole splitting that remains unchanged from 0.1 up to 0.4 Li inserted. Diffusion and/or passivation layer formation induces a decrease in Δ from 0.32 to 0.23 mm/s for 0.1 Li inserted into anatase. Beyond 0.5 Li inserted into the structure, we observe an increase in Δ, reflecting the progressive formation of a diffusion layer in the new orthorhombic phase, $Li_{0.5}$-TiO_2. Hence, tin plays as a local probe for Li insertion into TiO_2. Li insertion into sample B is composed of three steps:

(a) for $x < 0.07$, topotactic insertion into an anatase-like structure with formation of the diffusion/passivation layer partially reduces Sn^{IV} to Sn^{II}; (b) for $0.07 < x \leq 0.5$, a typical plateau for a mechanism involving two phases during orthorhombic $Li_{0.5}TiO_2$ phase formation is reached; and (c) for $x > 0.5$, the shape of the curve can be influenced by the

(27) Chouvin, J.; Branci, C.; Sarradin, J.; Olivier-Fourcade, J.; Jumas, J. C.; Simon, B.; Biensan, P. *J. Power Sources* **1999**, *81*−*82*, 277.
(28) Chouvin, J.; Olivier-Fourcade, J.; Jumas, J. C.; Simon, B.; Biensan, P.; Madrigal, F. J. F.; Tirado, J. L.; Perez Vicente, C. *J. Electroanal. Chem.* **2000**, *494*, 136.
(29) Courtney, I. A.; Dunlap, R. A.; Dahn, J. R. *Electrochim. Acta* **1999**, *45*, 51.

crystallite sizes and substitution effects, and there is formation of a diffusion layer in $Li_{0.5+x}TiO_2$.

Conclusion

This work deals with a forefront subject in battery materials, as it provides interesting information on anatase TiO_2 electrodes for Li ion batteries. Mössbauer spectroscopy is a powerful technique for gaining a better understanding of the mechanism of the reactions taking place in lithium test cells. Special interest arises from discriminating between textural and doping effects on the electrochemical response.

The electrochemical insertion of Li into TiO_2 follows a three-step mechanism. The first step is a topotactic insertion into Li_xTiO_2 ($x < 0.07$) with a small distortion of the anatase structure. A two-phase mechanism is characterized by a plateau at a potential of 1.75 V. It corresponds to the formation of $Li_{0.5}TiO_2$. The third domain is a topotactic insertion into the orthorhombic lithium titanate $Li_{0.5+x}TiO_2$. The potential value is not affected by substitutions, but the reversible capacity of the first domain is limited by the mechanism and can be reduced. The third step is characterized by a solid-solution insertion mechanism. This domain is strongly dependent on crystallite sizes and can be extended by tin substitution and control of synthesis conditions. Li ion dynamics in TiO_2 anatase are influenced by sizing down nanoparticles. The tin-doped compound has an advantage because swelling is limited compared to that in conventional anatase TiO_2. X-ray diffraction and ^{119}Sn Mössbauer spectroscopy gave us valuable information about both long-range order and the local environment of tin in the studied compound.

Acknowledgment. The authors thank EC for funding (NEGELiA, Contract ENK6-CT-2000-00082). The authors are grateful to P. Biensan and C. Tessier from SAFT and J. Scoyer, A. Audemer, and S. Levasseur from UMICORE for their fruitful discussions.

CM051445V